Infrared Aluminum Metamaterial Perfect Absorbers for Plasmon-Enhanced Infrared Spectroscopy

Kai Chen, Thang Duy Dao, Satoshi Ishii, Masakazu Aono, and Tadaaki Nagao**

Matured surface chemistry and excellent chemical stability have enabled gold to become the material-of-choice for plasmonic sensing in both visible and infrared wavelength range. Here, successful surface functionalization of metamaterials made from a low-cost abundant plasmonic material, aluminum, with phosphonic acid and subsequent detection of the C=O vibration mode via surface-enhanced infrared absorption spectroscopy is demonstrated. The metamaterial consists of infrared perfect absorbers fabricated by colloidal lithography. Near perfect absorption is achieved at resonance wavelengths, which can be readily tuned by changing the diameters of the Al disk resonators, enabling excellent overlapping with the molecular vibration. Separately, the detection of a physically adsorbed protein layer on the Al metamaterial is also demonstrated. Surface functionalization with phosphonic acid provides various functional groups to the Al surfaces. Combined with tunable metamaterials, the work herein opens up great opportunities for Al-based plasmonic nanostructures for biochemical sensing applications.

1. Introduction

Plasmonic metal nanostructures hold great potentials for a wide range of applications such as plasmon-enhanced photocatalysis[1–4] and surface-enhanced spectroscopies.[5–10] In most cases, gold is still the plasmonic material-of-choice because of its excellent chemical stability and matured surface chemistry, which enables easy integration of Au nanostructures with other molecules or polymers. Proper surface functionalization of plasmonic nanostructures is thus critical for their applications for bio- and chemical-sensing. Despite the popularity of gold, aluminum (Al) has recently drawn considerable attentions as alternative plasmonic materials, especially in the UV wavelength range where gold is excluded due to the interband transitions.[11–14] Al is the third most abundant element in the earth's crust and has already seen a great deal of applications in our society, notably in CMOS. Although Al deteriorates in air and in aqueous environment due to sulfur contamination, the natural Al_2O_3 oxide layer, 3–5 nm in thickness, can act as a protecting layer. This Al_2O_3 layer can be readily increased by further oxidation to provide more robust protection with some sacrifice of the enhanced near field as the analyte is pushed further away from the Al surface.[15] In the infrared range, this sacrifice does not pose a serious problem as the near field is well extended from the Al surface. Thus, exploring the feasibility of employing Al nanostructures for infrared biochemical sensing is of great interests for expanding the capabilities of Al plasmonic nanostructures.[16]

For biochemical sensing in the infrared range, surface-enhanced infrared absorption spectroscopy (SEIRA) has shown great potentials evidenced in a variety of structure designs, among which metamaterial perfect absorbers (MPAs) show remarkable sensitivity.[6,17,18] MPAs employ subwavelength nanostructures to engineer the effective impedance of the device to achieve total (or perfect) absorption at certain wavelengths. Recently, they have received considerable attention due to their potentials for applications in selective thermal emitters and ultrasensitive sensing.[19–22] A variety of geometrical designs have been proposed and fabricated to achieve perfect or near perfect absorption in a broad wavelength range.[23–26] In particular, Zhang et al. demonstrated Al-based dual band MPA using a dielectric bilayer.[27] More recently, Ayas et al. demonstrated hierarchical MPAs using Al and Ag showing SEIRA and SERS activities, where the molecules are immobilized on the Ag nanoparticle surfaces.[28] For sensing applications with these nanostructures, it is critical to properly modify their surfaces with certain functional molecules to achieve reliable and repeatable performance. Phosphonic acid has been applied to a range of oxide surfaces, such as ZnO and Al_2O_3. As we reported here, combination of phosphonic acid with Al MPAs thus provides an effective means to employ Al nanostructures for potential cost-effective biochemical sensing applications.

Most of the nanostructures for MPAs were fabricated by conventional lithographic tools such as e-beam lithography (EBL). While EBL is compatible with complex nanostructure design, it is difficult to achieve large-area patterning. Alternatively, scalable colloidal lithography (CL) (also known as nanosphere lithography) has proven to be a versatile nanofabrication technique suitable for fabrication of large-scale plasmonic nanostructures.[29–34] Herein, we demonstrate fabricating large-area

Dr. K. Chen, Dr. T. D. Dao, Dr. S. Ishii, Dr. M. Aono, Dr. T. Nagao
International Center for Materials Nanoarchitectonics (MANA)
National Institute for Materials Science (NIMS)
1-1 Namiki, Tsukuba, Ibaraki 305-0044, Japan
E-mail: CHEN.Kai@nims.go.jp; NAGAO.Tadaaki@nims.go.jp
Dr. K. Chen, Dr. T. D. Dao, Dr. S. Ishii, Dr. M. Aono, Dr. T. Nagao
CREST, Japan Science and Technology Agency
4-1-8 Honcho, Kawaguchi, Saitama 332-0012, Japan

DOI: 10.1002/adfm.201501151

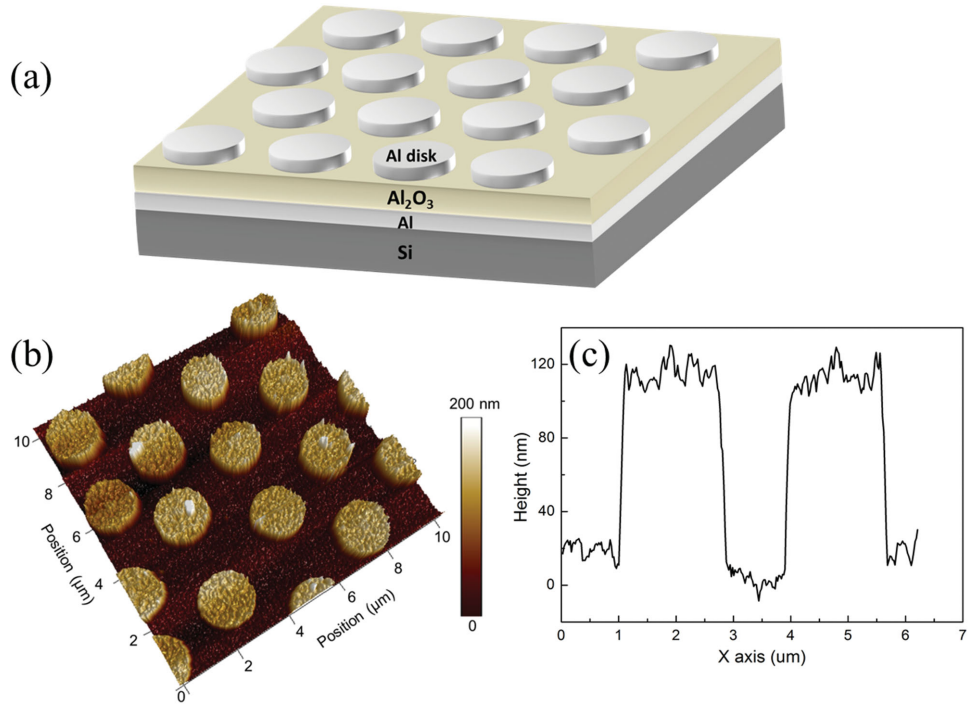

Figure 1. a) Schematic of the Al MPA in a conventional MIM configuration. b) Tilted view of the AFM image of the fabricated Al perfect absorber. c) Line-scan profile of the Al MPA along the dashed line in panel (b). The average height of the Al disk is ≈100 nm.

infrared Al MPAs using facile colloidal lithography and dry etching. The diameter of the Al disk resonators can be accurately controlled by oxygen (O_2) plasma etching time of the sphere masks and thus the resonance wavelength can be readily tuned. Subsequently, we functionalized the Al surfaces with phosphonic acid and successfully detected the characteristic C=O vibration band in the molecules with SEIRA. In addition, a physically adsorbed protein layer—bovine serum albumin (BSA)—was also detected with SEIRA on the Al MPAs.

2. Results and Discussions

Figure 1a illustrates the geometry of the Al metamaterial perfect absorber we used in a conventional metal–insulator–metal (MIM) geometry, where the top Al disk resonators and the bottom Al film are separated by an Al_2O_3 spacer layer. At resonance, the electric field of the incident electromagnetic field induces electric dipoles inside the Al disks while the magnetic field engenders magnetic dipoles in the MIM trilayers-antiparallel current running in the top Al disks and the bottom Al films. Thus the electromagnetic response of these MIM structures can be engineered to match their effective impedance with that of free space leading to zero reflection at certain wavelengths. Since the transmitted electromagnetic field is totally blocked by the bottom Al film, the combined effect of zero reflection and zero transmission result in total (or perfect) absorption by the structures at resonance wavelengths. Large field enhancement is expected at resonance wavelength of those Al disks providing an excellent platform for sensing applications.

Unlike previous reports, here the Al MPAs were fabricated using scalable nanofabrication techniques—colloidal lithography and dry etching—and thus large area sample preparation is possible without using sophisticated lithographic instruments. Figure 1b shows a representative atomic force microscopy (AFM) image of the fabricated Al perfect absorber. The Al disk arrays resemble the hexagonal pattern of monolayer of close-packed polystyrene spheres. Deviations from a perfect hexagonal arrangement exist in the Al disk arrays due to the combined effect of defects in the colloidal monolayers and heating during O_2 dry etching.[35] Our simulation shows that the optical properties of the structures are very robust against misalignment of the Al disks, which alleviates any strict requirement for precise fabrication (Figure S2, Supporting Information). Thus even though the periodicity of the pattern is not perfect, near perfect absorption can still be realized as we show in the following. The Al MPAs were patterned on a 1×1 cm^2 Si substrates and therefore the prepared samples are large enough to be easily characterized using conventional Fourier transform infrared (FTIR) instruments without the need of an IR microscope. The diameter of the Al disk can be easily tuned by controlling the etching time of the polystyrene spheres and the plasmon resonance wavelengths are accordingly tuned across a broad wavelength range (**Figure 2**).

Figure 2a shows the measured reflectance spectra of three Al MPA samples with different diameters of the Al disks, which were tuned by controlling the O_2 plasma etching time of the latex spheres as mentioned above. Longer etching time leads to smaller Al disks, which give rise to plasmon resonance at shorter wavelength (larger wavenumber). All the three samples exhibited near perfect absorption, ≈96%–97%, with the same

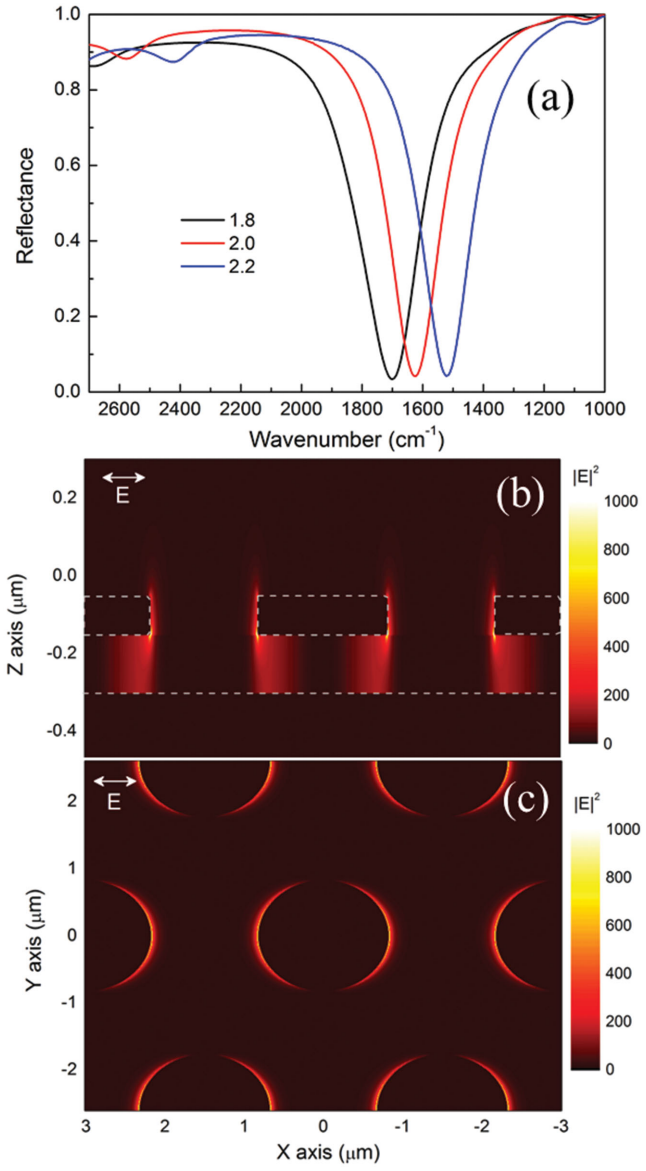

Figure 2. a) Measured reflectance spectra of three Al perfect absorbers with different disk diameters: 1.8, 2, and 2.2 μm. b) Cross-section view and c) top view of the simulated near-field profile of the electric field intensity $|E|^2$ at resonance for Al MPAs with disk diameters of 1.8 μm. The gray dashed line in panel (b) indicates the location of Al.

Al_2O_3 spacer layer thickness of 150 nm. The absorption efficiency is uniform over large areas of several hundreds of μm^2 (Figure S1, Supporting Information). Even larger areas can be achieved with monodisperse colloidal spheres and high-quality monolayers. As reported earlier,[6] the absorption efficiency does not show a strong dependence on the thickness of the spacer when it is near the optimum value for perfect absorption, which facilitates easier control over the plasmon resonance by simply changing the Al disk diameters without much concern for the thickness of the Al_2O_3 spacer layer. Thus, we can systematically tune the plasmon resonance peaks and accomplish excellent overlapping between the plasmon resonance and the molecular vibrational absorption considerably enhancing the signal-to-noise ratio. The shallow reflectance dips at the shorter wavelength (larger wavenumber) range are attributed to higher modes in the three Al MPA samples. Figure 2b displays the electric near-field intensity profile around the Al disk at the plasmon resonance wavelength demonstrating significantly enhanced electric field intensity around the Al disk rims (Figure 2c).

The popularity enjoyed by gold as plasmonic material is partially attributed to the matured surface chemistry. The strong Au–S bond, which has a similar bond strength as Au–Au bond,[36] has enabled surface functionalization of the gold surfaces with a great deal of chemical or biological entities leading to the wide use of gold in biochemical sensing applications.[37] Similarly, proper surface functionalization is also very important to Al nanostructures for their potential applications. Recently, phosphonic acid derivatives have been employed to modify metal oxide surface through the P–O–M (M: metal) bonds showing high stability and density.[38–40] Here, we functionalized Al MPA (with 1.8 μm Al disks) surfaces with 10-carboxydecylphosphonic acid (10-CDPA) and measured the reflectance spectra before and after the modification (**Figure 3**). Figure 3a shows the baseline-corrected absorbance spectra of the Al perfect absorber displaying the C=O vibration band of the COOH functional groups in 10-CDPA. The blue and red dashed lines represent the fitting curves to the two peaks and their sum, respectively. The absorption band can be fitted into two peaks at 1734 and 1767 cm^{-1}. It is known that the exact spectral position of the C=O vibration highly depends on the state of the COOH group: 1680–1710 cm^{-1} for hydrogen-bonded COOH and 1735–1760 cm^{-1} for free nonhydrogen-bonded COOH.[40,41] The 10-CDPA molecules were dissolved in water/IPA (1:1 volume ratio) mixtures and therefore hydrogen bonding is less likely due to the electrostatic repulsion between COOH. It is possible that the COOH group can interact with each other on the surface considering the long carbon chain of the molecule. For comparison, we also carried out surface functionalization on Al planar film with 10-CDPA. The Al film was deposited with e-beam evaporation instead of sputtering which is used for the fabrication of Al MPAs. Infrared reflection absorption spectroscopy (IRRAS) was used to collect the spectra from the Al film (Figure 3b). It is noted that the peaks in Figure 3a is ≈30 time stronger than those in Figure 3b corroborating the enhancement effect brought by the Al MPAs. The absorbance was measured at incident angle of 10° for Al MPAs while at grazing angle (≈80°) for Al films in IRRAS. Thus it is expected that the actual enhancement factor is much larger facilitating practical biosensing applications of such Al MPAs.

In Figure 3b, the absorption band can also be fitted with two peaks: 1747 and 1716 cm^{-1}, which is different from those of Al MPAs and could be due to different adsorption configurations of 10-CDPA on Al_2O_3 surfaces and different excitations. It is noted that the Al disks on the Al MPAs are formed by dry etching with BCl_3 and Cl_2 plasma. Although the Al disks are protected under the polystyrene spheres, the disk rims are directly exposed to the gases and residues are likely to accumulate on the plasma-bombarded rim surfaces, which are where the enhanced electric fields are located as shown in Figure 2b. These subtle differences between the two surfaces

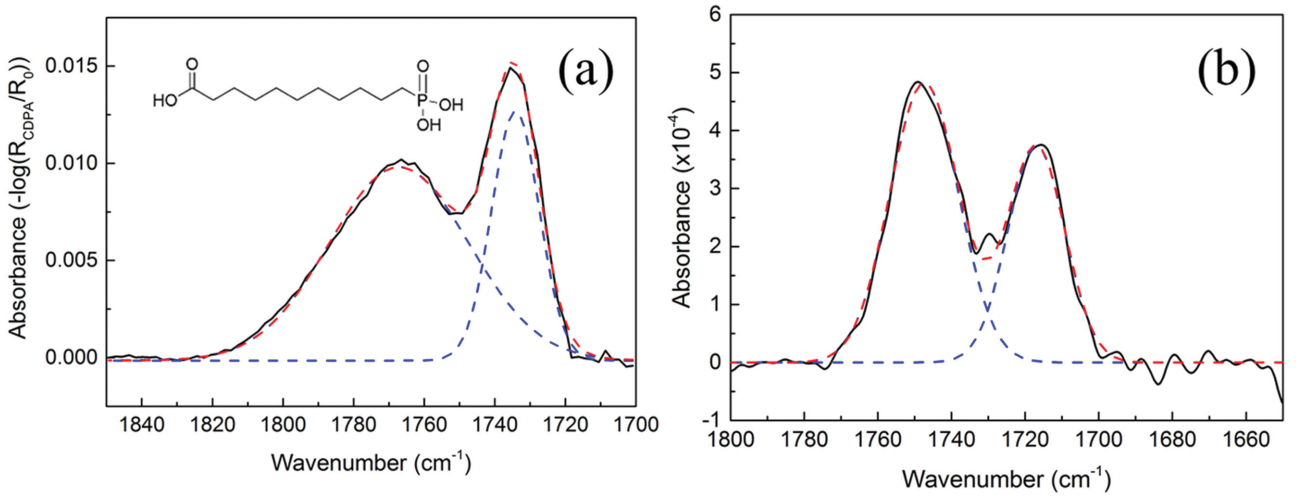

Figure 3. a) Absorbance spectrum of the C=O vibration bands in 10-CDPA immobilized on Al MPA. The spectrum is base-line corrected and the inset shows the molecular structure of 10-CDPA. b) IRRAS absorbance spectrum of 10-CDPA immobilized on Al film.

may contribute to the spectral difference observed between Figure 3a,b. In addition, only p-polarized light contributes to the signal in IRRAS while both p- and s-polarized light can interact with the molecules on Al MPAs at near-normal incidence (see the Experimental Section), which may also contribute to the observed spectral difference. The presence of other vibrational bands in the IRRAS spectrum also confirms the successful attachment of phosphonic acid to the Al film (Figures S3 and S4, Supporting Information).

The immobilization of 10-CDPA on the Al MPA surfaces was also investigated with X-ray photoemission spectroscopy (XPS) (**Figure 4**). Figure 4 shows the O1s and P2p spectra of the 10-CDPA coated on Al MPA. The O1s spectrum was fitted with Gaussian–Lorentz product containing five contributions to the peak: C–OH (535.5 eV), C=O (534.7 eV), P–OH (544.0 eV), P=O (533.2 eV), and Al–O (532.3 eV), which is consistent with previous report on phosphonic acid on ZnO.[40] The binding energy of the P2p component is located at 136 eV.

Therefore, successful surface functionalization of Al MPAs was demonstrated with phosphonic acid. It is noted that the molecule—10-CDPA—contains functional group COOH, which enables the substrates active for further biosensing with standard surface chemistry procedures, such as (1-ethyl-3-(3-dimethylaminopropyl)-carbodiimide)/*N*-hydroxysuccinimide (EDC/NHS) coupling, or through electrostatic interactions. Thus, the demonstrated surface functionalization, combined with the scalable nanofabrication techniques, opens up a new avenue for ultrasensitive biosensing with cost-effective Al plasmonic materials.

In the above, we demonstrated surface functionalization of Al MPAs with chemically adsorbed molecules. It is notable that the Al_2O_3 surfaces can also be functionalized by physical adsorption via hydrophobic or electrostatic interactions with functional molecules, such as proteins, providing additional means for surface functionalization for biosensing. We explored this possibility on Al MPAs with standard protein - bovine

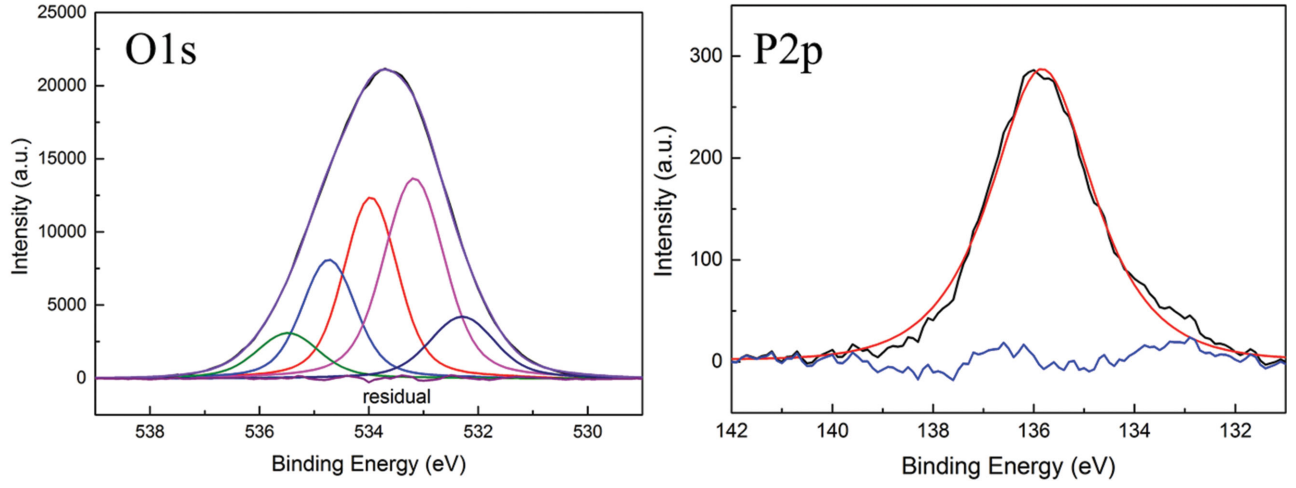

Figure 4. XPS spectra of 10-CDPA on Al MPA. Black curves are the background-corrected experimental peaks. Fitted peaks show good overlap with the measured curves.

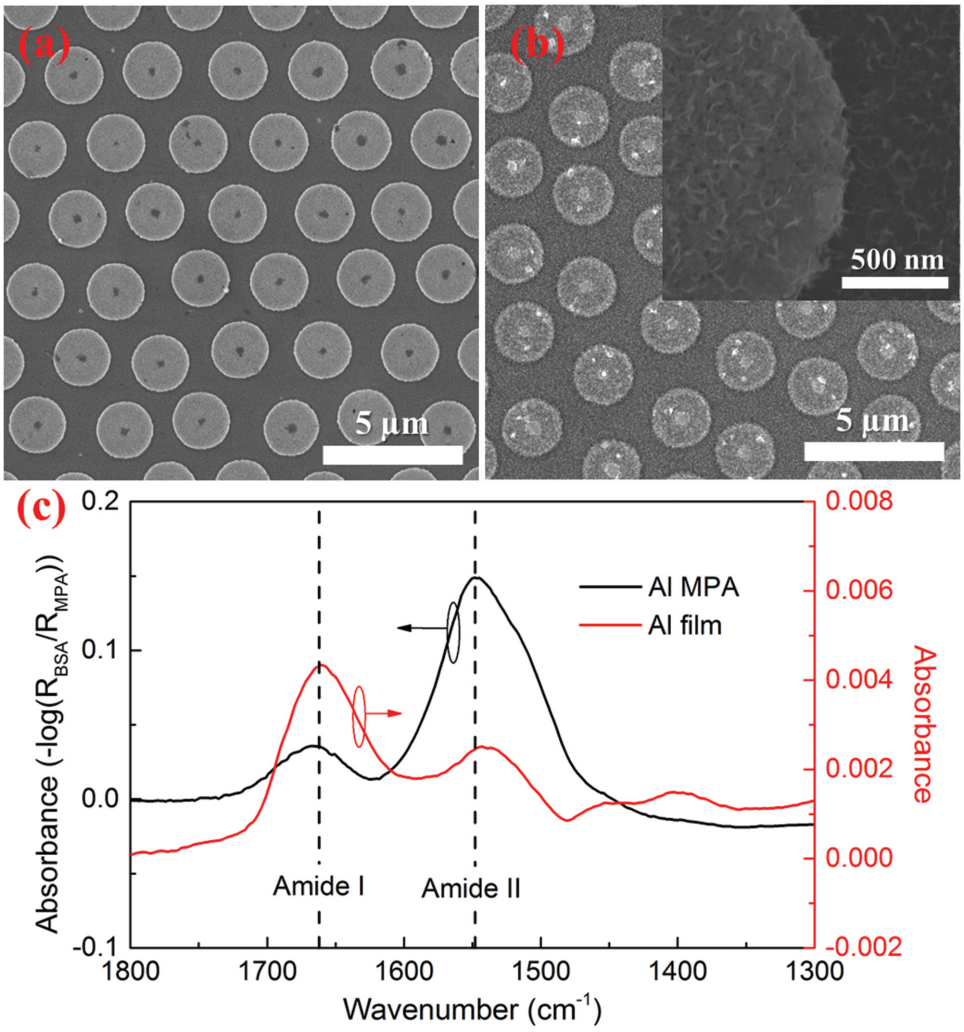

Figure 5. SEM images of Al MPAs a) before and b) after BSA molecules were physically adsorbed onto the surfaces. The inset in (b) shows the morphology of BSA on the oxide surfaces. c) Absorbance spectra of the BSA adsorbed on Al MPAs (black) and on Al planar film (red). The resonance of the MPA is overlapping with amide-II band.

serum albumin (BSA), which is expected to have amide bands located at ≈1660 cm^{-1} (amide-I) and ≈1550 cm^{-1} (amide-II) range just like other proteins (**Figure 5**). For this purpose, we again tune the diameters of the Al disks to overlap the resonance band with the amide-II band.

Figure 5a,b shows the SEM images of Al MPAs before and after BSA molecules physically adsorbed on oxide surfaces, respectively. It is likely that the BSA molecules physically self-assembled onto the surfaces via electrostatic interactions between positive charges on the native oxide Al_2O_3 layer and negative charges on the BSA molecules.[42,43] As shown in Figure 5b, BSA islands are also observed across the sample surface indicating that BSA multilayers occur during the process of physical adsorption. Figure 5c shows the absorbance spectra of the adsorbed BSA on Al planar film (red) as well as Al MPAs (black). In general, the two amide bands extracted from Al MPAs show higher values than those from Al film. Particularly, the amide-II band is ≈60 times larger and the amide-I band is ≈8 times larger, even though the amide-I band is stronger than amide-II for the case of Al film. This is attributed to the better overlapping of the plasmon resonance with the amide-II band demonstrating the spectral selectivity of the enhancement from Al MPA based SEIRA. Thus, Al MPAs provide an excellent platform for SEIRA biosensing readily tuning the plasmonic enhancement to the targeted vibrational frequency.

3. Conclusion

In summary, we have fabricated Al infrared metamaterial perfect absorbers with the scalable nanofabrication techniques colloidal lithography and dry etching. Compared with conventional nanofabrication techniques, such as e-beam lithography, the introduced method is scalable and wafer-scale production can be readily achieved. The MIM structure shows high tolerance for structural defects, such as disk misalignment, loosening the fabrication restrictions. The uniformity of the fabricated Al disks can be further improved with high-quality monolayers of spheres.

We demonstrated surface functionalization with phosphonic acid and subsequently performed plasmon-enhanced infrared spectroscopy utilizing the enhanced near field around the Al disks. We also showed physical adsorption of a BSA protein layer on the Al MPAs and selective plasmonic enhancement of the amide-II band from the protein. The plasmonic material and the nanofabrication technique demonstrated here enable large-area fabrication of low-cost metamaterials. Our work shows great potential of using Al as alternative plasmonic materials for infrared biosensing applications.

4. Experimental Section

Fabrication of Al MPAs: First, Al-Al_2O_3-Al films were sputtered (i-Miller CFS-4EP-LL, Shibaura) onto Si substrates with 100, 150, and 100 nm thicknesses, respectively. Polystyrene (PS) spheres (3 μm in diameter, Polysciences Inc.) were then self-assembled at water–air interface and transferred onto the multilayer films. Subsequently, the size of the PS spheres was reduced by inductively coupled plasma (ICP)-RIE technique using oxygen gas (20 sccm, antenna RF power 200 W, bias RF power 5 W, Ulvac CE-300I). With the etched PS spheres as mask, Al disks were formed by etching the top Al layer with gases BCl_3 and Cl_2 (3/3 sccm, antenna RF power 50 W, bias RF power 10 W). Finally, the PS spheres were removed by ultrasonication in toluene and ethanol.

Surface Functionalization: 10-carboxydecylphosphonic acid (10-CDPA) (Dojindo Molecular Technologies, Inc.) solution (2.5×10^{-3} M) was prepared in isopropyl alcohol (IPA)/water (1:1 volume ratio) mixtures. The Al MPAs and Al films were briefly cleaned with UV ozone (60 s) before immersion in the 10-CDPA solution for 72 h. Finally, the samples were taken out, cleaned with IPA and water and dried with nitrogen gas.

BSA Protein Sensing: Al MPA and Al films were treated under O_2 plasma (100 W, 30s) using a plasma asher (Mory Engineering Co. LTD) to remove any organic molecules contaminations. Then, the treated Al surface samples were soaked in to BSA aqueous solution (Sigma Aldrich, 1×10^{-3} M, pH = 6.9) for 24 h, and rinsed in distilled water and finally dried under a stream of nitrogen gas.

Characterization: The Al MPAs were characterized with a conventional FTIR spectrometer (Nicolet iS50R, Thermo Fisher Scientific Inc.). The reflectance spectra of the MPAs were collected using variable angle reflectance accessory (Harrick Scientific) with liquid nitrogen-cooled mercury cadmium telluride (MCT) detector. The incident angle of the light is fixed at 10°. The mapping of the resonance (Figure S1, Supporting Information) was done with a FTIR microscope (Nicolet Continuμm, Thermo Fisher Scientific Inc.) with near-normal incidence. The incident infrared light is limited by a 50×50 μm^2 aperture. The scanning area is 500×500 μm^2 with a scanning step of 20 μm and the sample was moved by a computer-controlled motorized stage. Infrared reflection absorption spectroscopy (IRRAS) was carried out with Smart Refractor accessory on the Al films. The collected spectra were baseline corrected and fitted with Gaussian curves. BSA adsorbed on an Al planar film was taken using ATR configuration (Nicolet IS50R FT-IR, DTGS-ATR detector and KBr beam splitter).

XPS analyses were performed using a Theta Probe (Thermo Fisher Scientific Inc.) equipped with a concentric hemispherical analyzer in the standard configuration. Spectra were acquired using a monochromatic Al Kα X-ray source operating at 100 W at a base pressure of 10^{-7} Pa. The measurements were conducted at takeoff angle of 53° with respect to the surface normal.

Simulation: The electric near-field profile of the Al MPAs was simulated using finite-difference time-domain (FDTD) method (FullWAVE, RSoft). The dielectric functions of Al and Al_2O_3 were taken from the literatures.[44,45] The grid size in the simulation was set to 5 nm.

Supporting Information

Supporting Information is available from the Wiley Online Library or from the author.

Acknowledgements

K.C. and T.D.D. contributed equally to this work.

Received: March 22, 2015
Revised: August 9, 2015
Published online: October 6, 2015

[1] L. Liu, S. Ouyang, J. Ye, *Angew. Chem. Int. Ed.* **2013**, *52*, 6689.
[2] X. Zhang, Y. L. Chen, R.-S. Liu, D. P. Tsai, *Rep. Prog. Phys.* **2013**, *76*, 046401.
[3] Y. Zhong, K. Ueno, Y. Mori, X. Shi, T. Oshikiri, K. Murakoshi, H. Inoue, H. Misawa, *Angew. Chem. Int. Ed.* **2014**, *53*, 10350.
[4] L. Liu, T. D. Dao, R. Kodiyath, Q. Kang, H. Abe, T. Nagao, J. Ye, *Adv. Funct. Mater.* **2014**, *24*, 7754.
[5] S. Aksu, A. E. Cetin, R. Adato, H. Altug, *Adv. Opt. Mater.* **2013**, *1*, 798.
[6] K. Chen, R. Adato, H. Altug, *ACS Nano* **2012**, *6*, 7998.
[7] C. V. Hoang, M. Oyama, O. Saito, M. Aono, T. Nagao, *Sci. Rep.* **2013**, *3*.
[8] H. Wang, J. Kundu, Naomi J. Halas, *Angew. Chem. Int. Ed.* **2007**, *46*, 9040.
[9] J. M. Hoffmann, X. Yin, J. Richter, A. Hartung, T. W. W. Maß, T. Taubner, *J. Phys. Chem. C* **2013**, *117*, 11311.
[10] F. Neubrech, S. Beck, T. Glaser, M. Hentschel, H. Giessen, A. Pucci, *ACS Nano* **2014**, *8*, 6250.
[11] M. W. Knight, N. S. King, L. Liu, H. O. Everitt, P. Nordlander, N. J. Halas, *ACS Nano* **2013**, *8*, 834.
[12] A. Taguchi, Y. Saito, K. Watanabe, S. Yijian, S. Kawata, *Appl. Phys. Lett.* **2012**, *101*, 081110.
[13] M. B. Ross, G. C. Schatz, *J. Phys. Chem. C* **2014**, *118*, 12506.
[14] D. O. Sigle, E. Perkins, J. J. Baumberg, S. Mahajan, *J. Phys. Chem. Lett.* **2013**, *4*, 1449.
[15] V. Canalejas-Tejero, S. Herranz, A. Bellingham, M. C. Moreno-Bondi, C. A. Barrios, *ACS Appl. Mater Interfaces* **2013**, *6*, 1005.
[16] O. Lecarme, Q. Sun, K. Ueno, H. Misawa, *ACS Photonics* **2014**, *1*, 538.
[17] A. Ishikawa, T. Tanaka, presented at *JSAP-OSA Joint Symp. 2014*, Sapporo, Hokkaido, Japan, September, **2014**.
[18] Y. Li, L. Su, C. Shou, C. Yu, J. Deng, Y. Fang, *Sci. Rep.* **2013**, *3*, 2865.
[19] X. Liu, T. Tyler, T. Starr, A. F. Starr, N. M. Jokerst, W. J. Padilla, *Phys. Rev. Lett.* **2011**, *107*, 045901.
[20] N. Liu, M. Mesch, T. Weiss, M. Hentschel, H. Giessen, *Nano Lett.* **2010**, *10*, 2342.
[21] J. A. Mason, S. Smith, D. Wasserman, *Appl. Phys. Lett.* **2011**, *98*, 241105.
[22] H. T. Miyazaki, T. Kasaya, M. Iwanaga, B. Choi, Y. Sugimoto, K. Sakoda, *Appl. Phys. Lett.* **2014**, *105*, 121107.
[23] Y. Avitzour, Y. A. Urzhumov, G. Shvets, *Phys. Rev. B* **2009**, *79*, 045131.
[24] M. K. Hedayati, M. Javaherirahim, B. Mozooni, R. Abdelaziz, A. Tavassolizadeh, V. S. K. Chakravadhanula, V. Zaporojtchenko, T. Strunkus, F. Faupel, M. Elbahri, *Adv. Mater.* **2011**, *23*, 5410.
[25] H. Wang, L. Wang, *Opt. Express* **2013**, *21*, A1078.

[26] J. Geldmeier, T. König, M. A. Mahmoud, M. A. El-Sayed, V. V. Tsukruk, *Adv. Funct. Mater.* **2014**, *24*, 6797.
[27] N. Zhang, P. Zhou, D. Cheng, X. Weng, J. Xie, L. Deng, *Opt. Lett.* **2013**, *38*, 1125.
[28] S. Ayas, A. E. Topal, A. Cupallari, H. Güner, G. Bakan, A. Dana, *ACS Photonics* **2014**, *1*, 1313.
[29] C. L. Haynes, R. P. Van Duyne, *J. Phys. Chem. B* **2001**, *105*, 5599.
[30] Y. Zheng, S. Wang, A. Huan, Y. Wang, *J. Non-Cryst. Solids* **2006**, *352*, 2532.
[31] G. Hong, C. Li, Q. Limin, *Adv. Funct. Mater.* **2010**, *20*, 3774.
[32] S. Yang, M. I. Lapsley, B. Cao, C. Zhao, Y. Zhao, Q. Hao, B. Kiraly, J. Scott, W. Li, L. Wang, Y. Lei, T. J. Huang, *Adv. Funct. Mater.* **2013**, *23*, 720.
[33] A. Dev, B. Dev Choudhury, A. Abedin, S. Anand, *Adv. Funct. Mater.* **2014**, *24*, 4577.
[34] R. Walter, A. Tittl, A. Berrier, F. Sterl, T. Weiss, H. Giessen, *Adv. Opt. Mater.* **2015**, *3*, 398.
[35] A. Plettl, F. Enderle, M. Saitner, A. Manzke, C. Pfahler, S. Wiedemann, P. Ziemann, *Adv. Funct. Mater.* **2009**, *19*, 3279.
[36] H. Hakkinen, *Nat. Chem.* **2012**, *4*, 443.
[37] K. Chen, H. D. Robinson, *J. Nanopart. Res.* **2011**, *13*, 751.
[38] L. B. Goetting, T. Deng, G. M. Whitesides, *Langmuir* **1999**, *15*, 1182.
[39] S. H. Brewer, D. A. Brown, S. Franzen, *Langmuir* **2002**, *18*, 6857.
[40] B. Zhang, T. Kong, W. Xu, R. Su, Y. Gao, G. Cheng, *Langmuir* **2010**, *26*, 4514.
[41] S. Pawsey, K. Yach, L. Reven, *Langmuir* **2002**, *18*, 5205.
[42] K. Rezwan, L. P. Meier, M. Rezwan, J. Vörös, M. Textor, L. J. Gauckler, *Langmuir* **2004**, *20*, 10055.
[43] K. Rezwan, A. R. Studart, J. Vörös, L. J. Gauckler, *J. Phys. Chem. B* **2005**, *109*, 14469.
[44] A. D. Raki, A. B. Djurisic, J. M. Elazar, M. L. Majewski, *Appl. Opt.* **1998**, *37*, 5271.
[45] E. D. Palik, *Handbook of Optical Constants of Solids*, Academic Press, Chestnut Hill, MA, USA **1998**.